A Bulk Silicon Dissolved Wafer Process for Microelectromechanical Devices

Yogesh B. Gianchandani, *Student Member, IEEE,* and Khalil Najafi, *Member, IEEE*

***Abstract*—A single-sided bulk silicon dissolved wafer process that has been used to fabricate several different micromechanical structures is described. It involves the simultaneous processing of a glass wafer and a silicon wafer, which are eventually bonded together electrostatically. The silicon wafer is then dissolved away to leave heavily boron doped devices attached to the glass substrate. The process requires a minimum of three masks: two for the silicon wafer to define the microstructures, and one for the glass wafer to define the interconnect between these devices. Overhanging features can be fabricated without any additional masking steps. It is also possible to fabricate elements with thickness to width aspect ratios in excess of 10:1. This paper describes measurements of various kinds of laterally driven comb structures processed in this manner, some of which are intended for application in a scanning thermal profilometer. They comprise shuttle masses supported by beams that are 160–360 μm long, 1–3 μm wide, and 3–10 μm thick. Some of the shuttles are mounted with probes that overhang the edge of the die by 250 μm. Resonant frequencies from 18 to 100 kHz, and peak-to-peak displacements up to 18 μm have been measured.**

I. Introduction

As part of the trend toward miniaturization of sensors and actuators and the development of complete microelectromechanical systems (MEMS), we have seen the evolution of many different kinds of technologies in recent years. A number of these technologies are based on surface micromachining of deposited films of polysilicon and/or other materials. Although surface micromachining is a versatile technique, it limits the maximum possible thickness of the microstructures to that of the deposited film [1]. Using chemical vapor deposition, for example, the microstructures can typically be made no more than 5 μm thick. This limitation can be circumvented by using electroplating techniques to make structures from metals. Molds for the electroplated metals can be made from PMMA-based photoresists patterned by specialized X-ray equipment [2]. They can also be made from photosensitive polyimides patterned by standard ultraviolet (G line) radiation [3]. Although microstructures with high aspect ratios have been demonstrated using electroplating techniques, special efforts are necessary to control the properties of the mechanical material. Bulk silicon micromachining [4]–[7] complements the capabilities of surface micromachining and electroplating techniques in that it allows MEMS of intermediate thickness to be fabricated from a well-controlled material, and in a manner compatible with standard IC processing. Microstructures amenable to bulk silicon micromachining include overhanging grippers, electrostatically driven motors, pressure sensors, valves, accelerometers, and resonant devices like diaphragms, beams, and bridges.

Research in bulk silicon mircomachining has proceeded along two tracks. One approach has been to grind and polish standard silicon wafers to define the thickness of the MEMS [4], [5]. This technique permits the fabrication of devices that may be as thick as the wafer itself. The substrate for these devices is another silicon wafer, which necessitates high temperature fusion bonding and infrared alignment. The other approach has been to use impurity based etch stops and dopant selective etchants to define the thickness of the MEMS, generally confining it to the range of 1–25 μm [6], [7]. In this technique the MEMS are usually bonded to a glass substrate that has been patterned with interconnect metal. Glass bonds to silicon at relatively low temperatures, and also permits optical alignment. In addition, it provides an insulating substrate that can be very beneficial in some applications. In [6], the silicon wafer is first selectively etched by KOH to form the bond anchors of the device. Oxide-masked boron diffusions are then performed to define the body of the device before it is anodically bonded to the glass substrate and immersed in an etchant that consumes all the undoped silicon. Although thick structures are possible with this process, the minimum widths achievable are limited by diffusion to the same order as the thicknesses. In addition, the sloping sidewalls characteristic of the KOH etch are not conducive to lateral electrostatic actuation. The process described by Suzuki in [7] is similar, except that the devices are formed by dry etching narrow, vertical gaps within the boron diffused regions, thus allowing the fabrication of laterally driven bulk silicon microactuators.

This paper describes an extension and refinement of the selective etching approach to bulk silicon micromachining to address a broader range of MEMS applications than has been demonstrated in the past. The issues include mask count reduction, fabrication of overhanging features, and perhaps most significantly, the fabrication of microstructures that have thickness-to-width aspect ratios in excess of 10:1. Achieving high-aspect ratios requires not only careful control of the etch chemistry, but also

Manuscript received March 16, 1992; revised June 30, 1992. Subject Editor R. S. Muller. This work was supported by NSF Grant ECS-8915215.
The authors are with the Center for Integrated Sensors and Circuits, University of Michigan, Ann Arbor, MI 48109-2122.
IEEE Log Number 9203150.

1057-7157/92$03.00 © 1992 IEEE

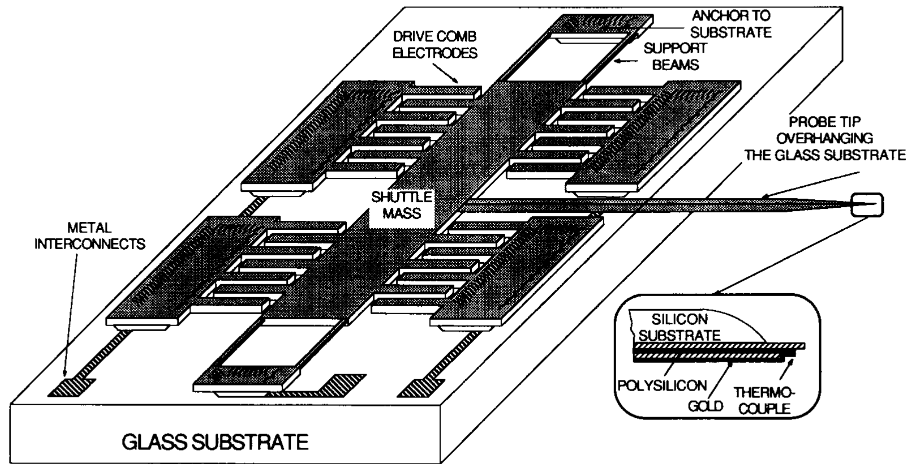

Fig. 1. Structure of the bulk Si scanning thermal profilometer.

special considerations regarding the layout of the etch mask. In Section II of this paper we discuss requirements imposed on the fabrication process by a variety of potential applications; in Section III we outline the process flow and the variations that are necessary to produce high aspect ratio structures; and in Section IV we describe the measured performance of the fabricated devices. Concluding remarks are provided in Section V.

II. Applications and Requirements

One application that we have targeted for this technology is a scanning thermal profilometer (STP) [8]. As we currently envision it, this device will consist of an overhanging probe connected to a laterally driven comb structure, which has a central shuttle mass supported by flexible beams (Fig. 1). At the tip of the probe will be a miniature thermocouple, and at its base will be electrical interconnects to control and readout circuitry, as well as provisions for heating the tip. As the tip is scanned over a sample, the thermocouple will sense temperature variations brought on by its varying proximity to features on the sample surface. The comb drives will be used to oscillate the probe, improving the noise immunity of the system. The nature of the application calls for a resonant frequency in the range of tens of kilohertz and for a thermally insulating substrate.

For the STP, as for most other flexure-based devices constrained to motion parallel to the substrate, there are arguments that motivate fabrication of high-aspect ratio elements. These devices typically have complementary requirements of vertical rigidity and lateral flexibility, which are best met by making the flexural elements thick and narrow. This follows from the fact that the moment of inertia of the flexible beams is proportional to hW^3 in the plane of motion and h^3W perpendicular to it, with h denoting the thickness and W the width of the beams. Vertical rigidity is desirable in these structures because it can improve the process yield and also reduce the likelihood of their clamping to the substrate. In addition, it contributes to the stability of device motion parallel to the substrate, which is important in many applications. In the case of the STP, for example, motion of the shuttle mass in any direction other than along the axis of the probe will reduce the spatial resolution of the scan. Another reason to increase the thickness of the MEMS is the corresponding increase in the sidewall capacitance of the driving and sensing ports. For applications in which electrostatic attraction between sidewalls is used as the propulsive force this enhances the driving power at a given voltage, and for those in which it is used as a measure (of position, for example), this enhances sensitivity. An example of the former type of device is the microgripper described in [9], and an example of the latter type is the ADXL-50 accelerometer recently announced by Analog Devices [10].

III. Fabrication Process

Since the primary structural concerns regarding the STP are the probe overhang, the device thickness, and the insulating substrate, the bulk silicon dissolved wafer process is particularly suitable for fabricating this device. The process used to fabricate planar microstructures uses three masks: one for a glass wafer that forms the substrate for the MEMS, and two for a silicon wafer from which the devices are micromachined. An extra (fourth) mask can optionally be used for the silicon wafer if structures of varying thickness are desired. The wafers are initially processed separately, then electrostatically bonded together and immersed in ethylene diamine pyrocatechol (EDP) to dissolve away undoped silicon, leaving heavily boron doped microstructures attached to the glass substrate. Electrical contact to the MEMS and interconnect between them is established using a layer of metal patterned onto the glass substrate prior to electrostatic bonding. The process flow is illustrated in Fig. 2.

We start by recessing with a KOH etch the entire top

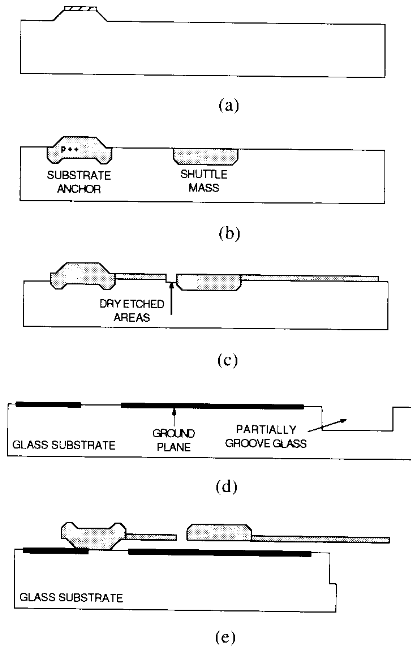

Fig. 2. Fabrication sequence for the bulk silicon dissolved wafer process. (a) Etch recess in silicon using KOH. (b) Perform deep boron diffusion to create anchor and shuttle mass (optional). (c) Perform unmasked shallow boron diffusion. Pattern using reactive ion etching to define beams, combs, and the probe. (d) Recess glass, pattern glass metallization using liftoff, partially groove glass to define overhang and dicing areas. (e) Electrostatically bond silicon and glass wafers, dissolve undoped silicon in EDP, separate dice by breaking along grooved lines.

surface of a standard Si wafer, except areas that will later be bonded to the glass substrate to anchor the MEMS. The depth of the recess (about 3 μm) determines the separation between the underside of the silicon microstructures and the top surface of the glass substrate. The sidewalls of the recess need not be vertical. This etch may also be performed by reactive ion etching (RIE), but caution must be exercised to ensure that the trench bottom is smooth, or subsequent processing will be adversely affected. In RIE smooth etch surfaces are generally associated with low pressures. We have used SF_6 and O_2 at 7–40 mtorr and 85 mW/cm^2 for this step with good results, but we find that the KOH etch yields even smoother trench bottoms, and may be necessary for some applications.

Next, the silicon wafer may optionally be subjected to a boron diffusion to define the thickest regions of the MEMS. This is necessary only in designs that call for structures of varying thickness. We typically diffuse to a depth of 15 μm at 1175°C, using a native oxide mask. We have used this step to fabricate bossed shuttle masses and beam anchors on some of our comb driven structures.

The next step is to perform an unmasked boron diffusion (1–25 μm deep) which defines the thickness of the planar (unbossed) structures like the probes. We also use this step to define the thickness of the beams and the teeth of the combs. These features are patterned by dry etching trenches that cut entirely through the boron diffused regions. Although the sidewalls of the trenches must be smooth and vertical, roughness in the trench floors is permissible because they terminate in undoped silicon which will be dissoved away in a later step. This etch is critical to the aspect ratios achievable with the dissolved wafer process, and will be discussed at length later. Following this etch the silicon wafer is stripped of the masking material and prepared for electrostatic bonding.

The glass (#7740 Corning) wafer is processed concurrently with the silicon wafer. A single mask is used to recess the top surface of the glass under the interconnect, and then to pattern the interconnect itself. First, a positive photoresist is spun on and patterned. The wafer is then immersed in BHF to recess the interconnect regions by 1200 Å. The etch rate of #7740 glass in BHF is about 340 Å/min. About 200 Å of Ti and 1500 Å of Pt are then evaporated on the wafer. The metal is lifted off from the field regions when the photoresist is removed. This method of processing the glass wafer saves one mask over previously reported techniques [7]. At the same time it permits more flexibility in selecting the thickness of the metal routed under the contact regions. The depth of the recess in the glass is such that the metal interconnect protrudes less than 500 Å above the field surface. The height of this protrusion is small enough to prevent the glass and silicon from being pushed apart as the bonding proceeds, and large enough to ensure a good ohmic contact between the device and the interconnect. A resistance of 12 Ω is typical for a 13 000 μm^2 contact area. This is adequate for most electrostatically operated devices, particularly because they do not sustain any direct current.

Once it has been recessed and patterned with the interconnect, the glass wafer is grooved in the regions where overhanging structures are desired and along scribe lines in between the dice. We have found that by leaving about 150–200 μm of glass in the grooves, the dice can easily be snapped apart individually, yet a 3 in wafer retains sufficient physical stength to survive the remaining steps in the fabrication process. This step permits us to achieve overhanging features without the use of an additional mask, which would add to turnaround time and wafer cost [9].

The grooved glass wafer is subjected to a pre-bond organic clean, aligned and electrostatically bonded to the Si wafer. The interface is maintained at about 400°C while 1000 V are applied across it for 15–30 min. The bonding temperature is well below the softening point of the glass wafer used. If the mating surfaces are very smooth, it is possible to bond at even lower temperatures and in less time. Rough surfaces may call for bonding at higher temperatures, and although this is possible, it should be noted that 1) higher temperatures may lead to delamination of the metal interconnect, and 2) the thermal stresses built into the device are related to the difference between the operating temperature and the bonding temperature, and the bond regions must be large enough to sustain these forces. A practical limit to the bonding temperature is

about 500°C because the thermal expansion coefficients of #7740 glass and silicon, which are very similar at room temperature, diverge rapidly above 500°C.

The bonded glass-silicon sandwich is then immersed in ethylene diamine pyrocatechol (EDP) to dissolve away the undoped silicon, leaving the boron doped MEMS mounted on the glass substrate [6]. Overhanging features are created wherever doped silicon regions extend past the grooved edges of the glass. We have observed that during the EDP dissolution the interconnect increases its protrusion above the field regions by about 2000 Å. Futhermore, possibly because of the corruption of poorly formed electrostatic bonds during EDP dissolution, a rapid thermal anneal at 600°C for 30 s is sometimes necessary to ensure ohmic contact between the devices and the metal interconnect underlying them [11].

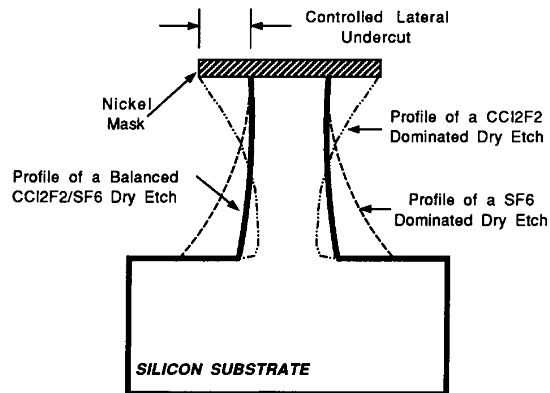

Fig. 3. Illustration of the different sidewall profiles using RIE chemistries based on SF_6 and CCl_2F_2 gases.

Reactive Ion Etching of High Aspect Ratio Microstructures

As mentioned previously, the etch that defines the micromechanical elements after the unmasked boron diffusion is critical in determining the final aspect ratios of the structures. In order to fabricate high aspect ratio structures this etch must satisfy a number of requirements: 1) it must produce trenches with smooth, vertical sidewalls; 2) it must be fast enough to achieve the desired depths in an acceptable time; 3) it must function with a masking material that can be patterned into fine geometries and be easily removed after the etch.

Dry etching of deep structures with fine features has long been of interest to the IC industry. Applications include electronic device isolation and the formation of trench capacitors for charge storage [12]. Dry etching has also been used for the micromachining of silicon [7], [13]. The most promising chemistries for RIE appear to be those based on gases with Cl and F as components. For example, mixtures of C_2ClF_5 and SF_6 have been known to produce deep trenches with vertical sidewalls when used in combination with a resist mask. This etch is sensitive to the mask used. It is believed that polymer formation on the sidewalls, in which the resist participates, is instrumental in determining the trench profile [12], [13]. A disadvantage of this etch is that the thickness of the masking material, which may be several microns of photoresist or a combination of resist and SiO_2, is large enough to raise concerns about patterning fine geometries.

In order to define the micromechanical elements we performed RIE using SF_6 (20 sccm) and O_2 (15 sccm) at 7 mtorr pressure and 80 mW/cm^2 power. The bias voltage was -160 V. When a 2000 Å thick aluminium mask was used, these conditions yielded an etch rate of about 800 Å/min, subject for loading, for boron doped Si. The sidewall angles were 3°–6° off the vertical. (Raising the chamber pressure reduced the etch rate and increased the sidewall angles.) This etch was adequate for elements 2–3 μm wide and up to about 10 μm thick. In order to fabricate elements with a higher aspect ratio, however, it was necessary to use a faster and more vertical etch. One such etch is based on a mixture of SF_6 and CCl_2F_2 [12]. We found that these gases have complementary effects on the trench profile, permitting some flexibility in tailoring the sidewalls. As shown in Fig. 3, dominance of SF_6 causes the bottom of the trench to be narrower than the top, whereas the dominance of CCl_2F_2 has the opposite effect, resulting in re-entrant profiles. When the effects of these gases are balanced, near-vertical trench sidewalls can be achieved despite the undercut. Our results were obtained in a reactor with a plate diameter of 30 cm, under 50 mTorr pressure and 300 W power. The bias voltage was -310 V, the flow rate of SF_6 was 20 sccm, and CCl_2F_2 was varied between 10–12 sccm, depending on the targeted etch depth. (This variation was necessary to control the bowing of the sidewalls.) We found that under these conditions, heavily boron doped Si was etched at about 1400 Å/min in the vertical direction, with lateral undercut, determined primarily by the SF_6 content of the gas mix, proceeding at 13% of that rate. A 1000 Å thick nickel mask was used with this etch. The sidewalls of the trenches were smooth insofar as permitted by the mask edge definition, but the floors were rough. Smoothness of the sidewalls is important in the fabrication of micron-width beams. As mentioned before, however, roughness of the trench floors is of no consequence in this step because the etch traverses the entire thickness of the boron diffusion, terminating in material that is later dissolved in EDP.

A final note on etching is in relation to the dependence of the etch rate on the feature size. As documented in [14], the etch rate reduces as the depth of the trench exceeds its width. For example, regions around the beams of the laterally driven comb structures will normally be etched more quickly than the gaps between the drive combs, thus causing greater undercutting of the beams. To control this phenomenon we used *etch buffers*, allowing only 2 μm wide trenches to be etched on either side of the beams, as shown in Fig. 4. (The 13% lateral undercut described above for the SF_6 and CCl_2F_2 mix was

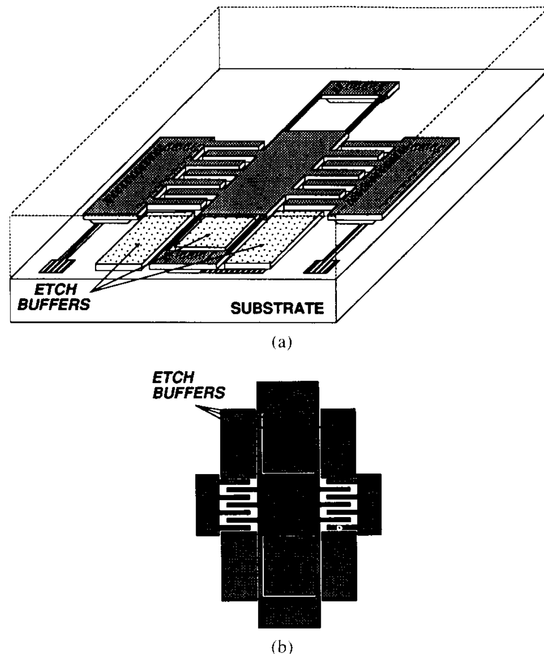

Fig. 4. (a) The flexible support beams of the laterally driven resonators are defined by etching narrow trenches on either side of them. The unetched regions, called etch buffers, help to control the RIE, and float away during EDP dissolution. (b) A top view of the RIE mask showing the etch buffers.

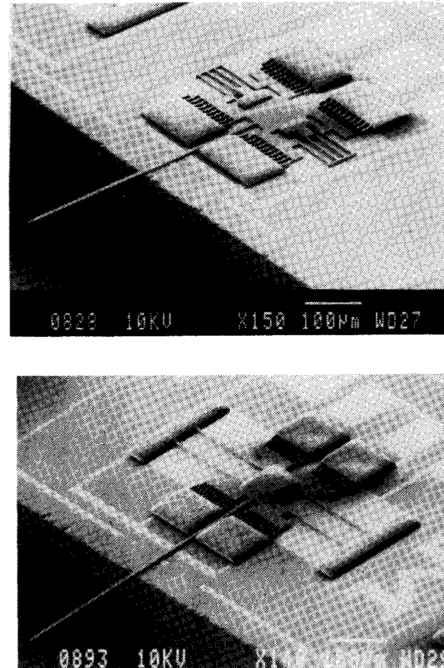

Fig. 5. SEM photographs showing two kinds of laterally driven comb structures with overhanging probes.

obtained in 2 μm wide trenches.) The etch buffers are not attached to any bond anchors and float away during EDP dissolution. They do not obstruct device movement. The buffers ensure that 1) the variation in the vertical and lateral etch rates remains uniform across the die and the wafer as the trenches deepen, and 2) the localized loading of the plasma, in the sense of consumption and generation of the reactant species and products, is also uniform. Although we have not compiled any statistical data on the RIE step in this process, our experience shows that etch buffers are particularly helpful in the machining of thick and narrow structures.

IV. Experimental Results and Discussion

Three kinds of laterally driven comb resonators with overhanging probes were fabricated and tested: folded beam with planar shuttle mass (lat1), straight beam with planar shuttle mass (lat2), and straight beam with bossed shuttle mass (lat3). The structures had probes extending from their shuttle masses, overhanging the edge of the glass substrate by about 250 μm. There were metal ground planes beneath the beams and shuttle masses to minimize damping of the motion from parasitic capacitive effects. The effective beam lengths were 200 μm in all three cases. Fig. 5, which includes the SEM photographs of lat1 and lat3, shows that free-standing devices with well-defined edges and multiple thicknesses can be achieved. Two separate sets of devices were fabricated—one with 3.7 μm thick beams and the other with 6.4 μm thick beams. The same mask was used in the RIE step for both sets, which called for trenches of different depths. This meant that the beams for the two sets were undercut by different amounts, causing the effective beams widths to be unequal. In general, however, it is expected that such sharing of masks will not be necessary, and that the masks can be designed to compensate for the undercut associated with the selected RIE recipe.

We also fabricated laterally driven comb resonators without overhanging probes in 5 and 10 μm thicknesses (Fig. 6). The effective beam lengths of these devices varied from 160 to 360 μm, and the beamwidths were 2.15 and 1.3 μm for the 5 and 10 μm thick devices, respectively. The beamwidths and the gaps between the teeth of these devices differed with the thickness as explained above. Note that all the components of these structures, including the shuttle masses and the teeth, were fashioned from elements of width identical to the flexible beams. Fig. 7 shows a close-up of a 10 μm thick folded beam.

Using the RIE techniques discussed in Section III it is possible to fabricate elements with very narrow widths. Fig. 8 shows SEM views of the folded beams of the laterally driven device shown in Fig. 6. These beams are about 1 μm wide and 10 μm thick. Lateral undercut produced by the RIE can also be exploited to create submicron gaps without submicron processing [15]. Fig. 9 shows SEM views of a 5 μm thick laterally driven device and a magnified view of the drive combs. The layout of the combs is such that the edges of opposing teeth are collinear. The lateral undercut permits separation be-

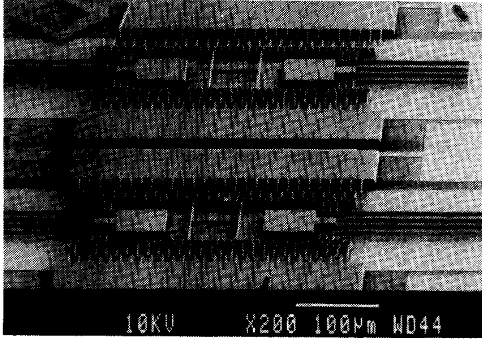

Fig. 6. SEM views of 10 μm thick laterally driven resonant devices without overhanging probes.

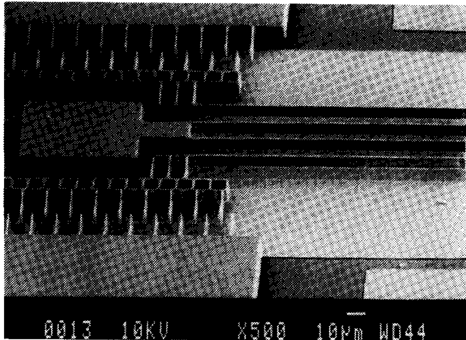

Fig. 7. A close-up SEM view of the 10 μm thick folded beams and drive combs of the laterally driven structures shown in Fig. 6.

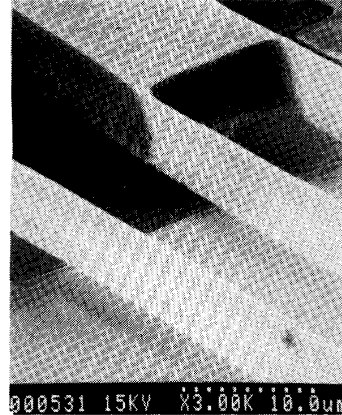

(a)

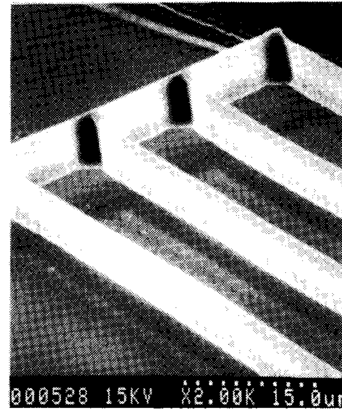

(b)

Fig. 8. Close-up views of the 10 μm thick folded beam in Fig. 7, showing (a) the area near the beam anchor, and (b) the area near the fold in the beam.

tween these edges to be < 1 μm when the device motion gains sufficient amplitude.

The laterally driven comb resonators described above were tested electrically by grounding the shuttle masses and driving the combs on one side of the device with a 0 to Vp square wave of varying period. Even at atmospheric pressure the quality factors (Q's) of the devices were high enough to filter out harmonics from the input signal, leaving the measurements near resonance unaffected. This was verified by measuring the resonant frequency of a few devices with a small ac signal riding on a larger dc bias, as described in [1]. The peak-to-peak deflections of the shuttles were estimated by visual inspection of the blurred region in the direction of motion.

Table I summarizes the measurements of all the folded beam devices, with and without overhanging probes. Folded beam devices are relatively free of internal stress, and their frequency response is typically as plotted in Fig. 10. The measured resonant frequencies of these structures varied from 18 to 100 kHz, and were independent of the measurement technique and the drive voltage used. All the measurements were done at room temperature and atmospheric pressure. The resonant frequency of the folded beam devices can be theoretically estimated using the following formula [16]:

$$\omega^2 = \frac{24\,E\,I}{L^3(M + 0.5\,M_S + 2.743\,M_L)}; \qquad I = \frac{hW^3}{12}$$

where E is the Young's modulus of the beam, I is its moment of inertia in the direction of the flexure, L is the length of each beam from the anchor to the fold (or from the fold to the shuttle mass), M_L is its mass, W is its width, M is the mass of the shuttle, and M_S is the mass of the stiffener at the fold of the beam. If the measured ω^2 is plotted against the calculated ω^2/E for devices with various beam widths and lengths, the slope of the best linear fit to the resulting scatter plot can be used to find the average value of E. This is done in Fig. 11, and E is found to be about 175 ± 40 GPa, with the error resulting primarily from uncertainty in measurements of the beamwidths from SEM photographs. This value is in general agreement with results obtained using a different measurement technique on similar material [17]. Note that in Fig. 11 the only measurement from Table I that does not closely approach the fitted line is for the 3.7 μm thick device. All other devices in this plot are at least 5 μm thick. If this single data point is used to find E for thin structures, the value obtained is 154 ± 40 GPa. Although more data are needed before any conclusions can be drawn, it is plausible that E differs for thinner structures

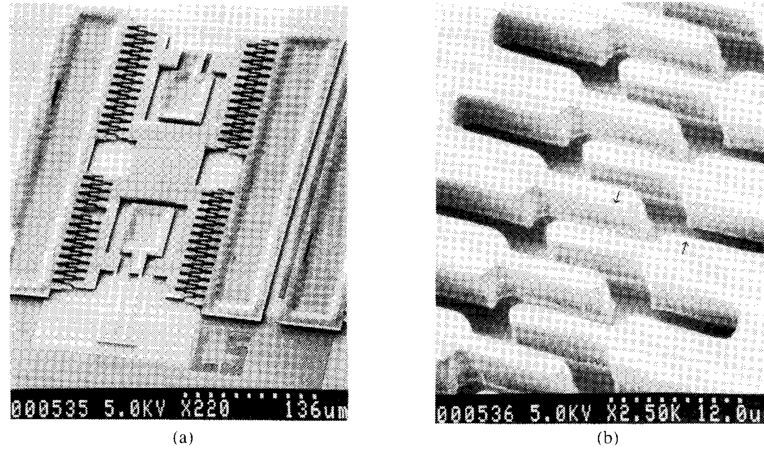

Fig. 9. SEM views of (a) a 5 μm thick laterally driven device with gaps between opposing comb teeth that are effectively submicron once motion is sufficiently large, and (b) a magnified view of the teeth with arrows indicating two proximal edges.

TABLE I
MEASUREMENTS OF FOLDED BEAM DEVICES

Device Name	Beam Length (μm)	Beamwidth (μm)	Beam Thickness (μm)	Plate Mass (10^{-9} g)	Beam Mass (10^{-9} g)	Stiffener Mass (10^{-9} g)	Resonant Frequency (kHz)	Q (approximate)
lat1A	200	2.58	3.7	239.8	2.22	2.50	44.4	114
lat1B	200	2.37	6.4	414.8	3.53	4.32	45.2	110
L9A	160	2.15	5	80.35	2.00	1.25	100	100
L9B	160	1.30	10	97.17	2.42	1.51	62.1	160
L10A	260	2.15	5	80.35	3.26	1.25	48.3	105
L10B	260	1.30	10	97.17	3.94	1.51	30.8	160
L11A	360	2.15	5	80.35	4.51	1.25	29.0	170
L11B	360	1.30	10	97.17	5.45	1.51	18.9	54

Note that the beamwidths were estimated from SEM photographs, and are accurate to about $\pm 10\%$. The resonant fequency measurements are accurate to ± 0.05 μs. The Q was visually estimated at atmospheric pressure; its values are to be used as guidelines only, not as exact measurements.

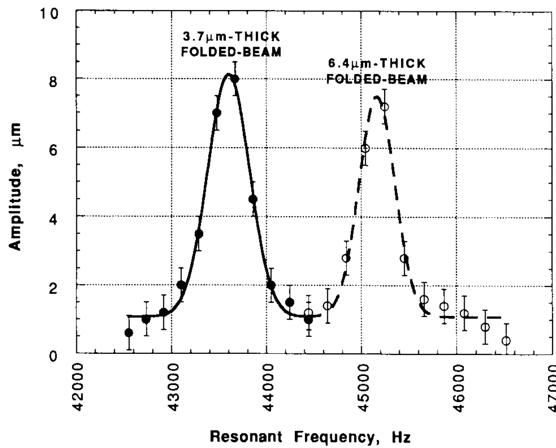

Fig. 10. Typical frequency response curves for folded beam (lat1) structures measured near fundamental resonance at atmospheric pressure.

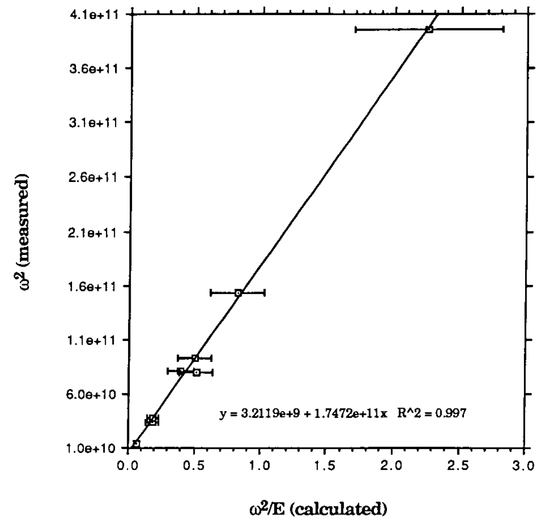

Fig. 11. The square of the measured resonant frequencies (ω^2) of the folded beam devices are plotted against the calculated ω^2/E. The slope of the best linear fit to the resulting scatter plot provides the average value of E. The primary source of error is from measurements of the widths of the flexible beams of the devices. From this plot, $E = 175 \pm 40$ GPa.

because of varying degrees of structural change experienced by the silicon lattice as boron diffusion progresses [18].

Unlike folded beam devices, straight beam structures

TABLE II
MEASUREMENTS OF STRAIGHT BEAM DEVICES WITH FLAT (lat2) AND BOSSED (lat3) SHUTTLE MASSES

Device	Thickness (μm)	Beamwidth (μm)	Plate Mass (kg)	Average Measured Res. Freq.	Intrinsic Stress
lat2	3.7	2.58	2.40×10^{-10}	30.6 kHz	18.5 ± 4 MPa
lat2	6.4	2.37	4.15×10^{-10}	28.8 kHz	18.5 ± 4 MPa
lat3	3.7	2.58	5.26×10^{-10}	21.4 kHz	18.5 ± 4 MPa
lat3	6.4	2.37	6.66×10^{-10}	23.5 kHz	18.5 ± 4 MPa

The layout dimensions of each beam are 200 μm total length. The mass of the beams is negligible compared to the plate mass in these designs.

(lat2, 3) are not free of internal stress. The primary sources of internal stress are 1) the expansion mismatch between the silicon and glass wafers during electrostatic bonding, and 2) the inherent stress in the silicon elements caused by the boron diffusion. The beams are additionally stressed by the motion of the shuttle mass, causing the frequency responses to exhibit hysterisis [16]. Resonant frequencies of these devices are therefore measured at low excitations, with < 1 μm peak-to-peak motion. The values obtained for the fabricated devices ranged from 18 to 33 KHz. Using the values of Young's modulus derived from the folded beam structures, the internal stress in the straight beams of lat2 and lat3 can be calculated. This analysis yields 18.5 ± 4 MPa, which is in agreement with previous reports [17]. The measurements of the straight beam devices are summarized in Table II.

We have performed experiments to study the degradation of bulk silicon comb resonators over extended exercise periods. A device of the type L11B (Table I), with 10 μm thick and 360 μm long beams was resonated for 17.6 h at about 8 μm peak-to-peak amplitude. This amounts to more than 920 million cycles with a maximum stress of about 84 MPa from the beam curvature. There was no perceptible change in the resonant frequency after this test. Since the frequency measurements were accurate to the closest 0.1 μs, this indicates a change of less than 0.1%, if any. A device of the type L11A (Table I) with 5 μm thick and 360 μm long beams was exercised at 8 μm peak-to-peak amplitude (139 MPa maximum stress) for more than 13.6 billion cycles, once again with imperceptible ($<0.15\%$), if any, change in resonant frequency. In both cases, the devices were operating normally when the tests were terminated. These initial results suggest that bulk silicon boron doped devices can sustain large amplitude motion over long periods of time without degradation. A more accurate and detailed study is under way.

In summary, the measurements of the devices indicate that desired resonant frequencies can be achieved accurately and reproducibly. The devices have high Q and no perceivable motion perpendicular to the plane of excitation. By all indications, therefore, bulk silicon micromachined devices are suitable for application in the scanning thermal profilometer as well as in many other micromechanical devices.

V. CONCLUSION

We have proposed and demonstrated the feasiblity of a simple, high yield, single-sided, three mask process for fabricating microelectromechanical structures from boron doped bulk silicon. Structures with varying thicknesses have been fabricated with the help of an additional mask, and overhanging features have been achieved at essentially no cost. Features with thickness-to-width aspect ratios of about 10 : 1 have been fabricated with the help of a new approach to RIE mask design and carefully selected RIE conditions. A new technique has also been developed to pattern the interconnect and perform lead transfer using only one mask. Many kinds of structures have been fabricated with this technology, including cantilevers, bridges, microgrippers, and laterally driven resonant structures with straight and folded beams. The laterally driven resonant structures, with beams varying from 160–360 μm in length, 1–3 μm in width, and 3–10 μm in thickness have been tested extensively. Measurements of these devices demonstrate that high frequency, high Q, large amplitude motion can be sustained in a stable manner over extended periods of vigorous excitation. The resonant frequencies of these devices range from 18–100 KHz, the Q values are typically greater than 100 at atmospheric pressure, and vibratory amplitudes as high as 18 μm peak-to-peak have been observed. The devices have been tested for more than 13.6 billion cycles of large amplitude motion without any signs of degradation. The Young's modulus for heavily boron doped single crystal silicon and intrinsic stress in the material have been derived from these measurements, and are found to be in agreement with previously published values.

ACKNOWLEDGMENT

The authors gratefully acknowledge the contributions of Mr. Jeffrey Fournier, Ms. Terry Hull and Mr. Arjun Selvakumar to the processing effort, and of Mr. Hassen Hammoud to the mechanical design considerations. We thank Dr. George Hazelrigg of the National Science Foundation for his support and encouragement.

REFERENCES

[1] W. C. Tang, T. C. H. Nguyen, and R. T. Howe, "Laterally driven polysilicon resonant microstructures," *Sensors and Actuators*, vol. 20, pp. 25-32, 1989.

[2] H. Guckel, T. R. Christenson, K. J. Skrobis, D. D. Denton, B. Choi, E. G. Lovell, J. W. Lee, S. S. Bajikar, and T. W. Chapman, "Deep X-ray and UV lithographies for micromechanics," in *Tech. Dig. Solid-State Sensors and Actuators Workshop*, Hilton Head, SC, June 1990, pp. 116-122.

[3] A. B. Frazier and M. G. Allen, "High aspect ratio electroplated microstructures using a photosensitive polyimide process," in *Proc. IEEE Workshop on Microelectromech. Syst.* (MEMS '92), Travemünde, Germany, Feb. 1992, pp. 87-92.

[4] K. Petersen, D. Gee, F. Pourahmadi, R. Craddock, J. Brown, and L. Christel, "Surface micromachined structures fabricated with silicon fusion bonding," in *Proc. Int. Conf. Solid-State Sensors and Actuators* (Transducers '91), San Francisco, CA, June 1991, pp. 397-399.

[5] K. Petersen, F. Pourahmadi, J. Brown, "Resonant beam pressure sensor fabricated with silicon fusion bonding," in *Proc. Int. Conf. Solid-State Sensors and Actuators* (Transducers '91), San Francisco, CA, June 1991, pp. 664-667.

[6] H. L. Chau and K. D. Wise, "An ultraminiature solid-state pressure sensor for a cardiovascular catheter," *IEEE Trans. Electron Devices*, vol. 35, pp. 2355-2362, Dec. 1988.

[7] K. Suzuki, "Single-crystal silicon micro-actuators," in *Tech. Dig. IEDM*, San Francisco, CA, Dec. 1990, pp. 625-628.

[8] H. K. Wickramasinghe, "Scanned-probe microscopes," *Scientific Amer.*, pp. 98-105, Oct. 1989.

[9] C. J. Kim, A. P. Pisano, and R. S. Muller, "Silicon-processed overhanging microgripper," *J. Microelectromech. Syst.*, vol. 1, pp. 31-36, Mar. 1992.

[10] F. Goodenough, "Airbags boom when IC accelerometer sees 50G," *Electron. Design*, Aug. 8, 1991.

[11] J. Ji, Univ. Michigan, personal communication, Nov. 1991.

[12] J. P. McVittie and C. Gonzales, "Anisotropic etching of Si using SF_6 with C_2ClF_5 and other mixed halocarbons," in *Proc. Fifth Symp. Plasma Processing*, G. S. Mathad, G. C. Schwartz, and G. Smolinsky, Eds. Electrochem. Soc., vol. 85-1, pp. 552-567.

[13] C. Linder, T. Tschan, and N. F. de Rooij, "Deep-dry etching techniques as a new IC compatible tool for silicon micromachining," in *Proc. Int. Conf. Solid-State Sensors and Actuators* (Transducers '91), San Francisco, CA, June 1991, pp. 524-527.

[14] Y. H. Lee and Z. H. Zhou, "Feature-size dependence of etch rate in reactive ion etching," *J. Electrochem. Soc.*, vol. 138, no. 8, pp. 2439-2445.

[15] T. Furuhata, T. Hirano, K. J. Gabriel, H. Fujita, "Sub-micron gaps without sub-micron etching," in *Proc. IEEE Microelectromech. Syst.*, (MEMS'91), Nara, Japan, Feb. 1991, pp. 57-62.

[16] R. I. Pratt, G. C. Johnson, R. T. Howe, and J. C. Chang, "Micromechanical structures for thin film characterization," in *Proc. Int. Conf. Solid-State Sensors and Actuators* (Trandsucers '91), San Francisco, CA, June 1991, pp. 205-208.

[17] K. Najafi and K. Suzuki, "A novel technique and structure for the measurement of intrinsic stress and Young's modulus of thin films," in *Tech. Dig. IEEE Microelectromech. Syst. Workshop*, Salt Lake City, UT, 1989, pp. 96-97.

[18] X. J. Ning, P. Pirouz, M. Mehregany, and W. Chu, "Cross-sectonal TEM studies of heavily boron doped silicon," in *Proc. Int. Conf. Solid-State Sensors and Actuators*, San Francisco, CA, June 1991, pp. 755-758.

[19] Y. Gianchandani and K., Najafi, "A bulk silicon dissolved wafer process for Microelectromechanical systems," in *Dig. Int. Electron Devices Meet.*, Washington, DC, Dec. 1991, pp. 757-760.

[20] ——, "Micron-Sized, high aspect ratio bulk Silicon Micromechanical Devices," in *Proc. IEEE Workshop on MicroElectroMech. Syst.* (MEMS '92), Travemünde, Germany, Feb. 1992, pp. 208-213.

[21] ——, "Batch fabrication and assembly of micromotor-driven mechanisms with multi-level linkages," in *Proc. IEEE Workshop on Microelectromech. Syst.*, (MEMS '92), Travemünde, Germany, Feb. 1992, pp. 141-146.

Yogesh B. Gianchandani (S'83-M'85-S'90) received the B.S. degree from the University of California, Irvine, in 1984, and the M.S. degree from the University of California, Los Angeles, in 1986, both in electrical engineering. He is currently a Ph.D. candidate in electrical engineering at the University of Michigan, Ann Arbor.

From 1985 to 1989 he was emplolyed as a circuit designer first by Xerox Corporation, El Segundo, CA, and then by Microchip Technology, Chandler, AZ. His work forcused on digital CMOS integrated circuits at both locations. His research interests include the design and fabrication of integrated sensors and actuators, and supporting circuitry.

Mr. Gianchandani is a member of Eta Kappa Nu and Tau Beta Pi.

Khalil Najafi (S'84-M'85) was born in 1958. He received the B.S.E.E. and M.S.E.E. degrees, both with highest honors from the University of Michigan, Ann Arbor, in 1980 and 1981, respectively, and the Ph.D. degree in electrical engineering from the University of Michigan, Ann Arbor, in 1986.

From 1986 to 1988 he was employed as a Research Fellow, from 1988 to 1990 as an Assistant Research Scientist, and since 1990 as an Assistant Professor in the Department of Electrical Engineering and Computer Science, University of Michigan. His research interests include the development, design, fabrication, and testing of: solid-state integrated sensors and microactuators; analog and digital integrated circuits; implantable microtelemetry systems and transducers for biomedical applications; technologies and structures for micro electromechanical systems and microstructures; and packaging techniques for implantable microtransducers.

Dr. Najafi was the recipient of the Beatrice Winner Award for Editorial Excellence at the 1986 International Solid-State Circuits Conference, and of the Paul Rappaport Award for co-authoring the Best Paper published in the IEEE TRANSACTIONS ON EELECTRON DEVICES for the year 1990. He is an Associate Editor for the *Journal of Micromechanics and Microengineering*, and is a member of Tau Beta Pi, Eta Kappa Nu, and Electrochemical Societies.